

# Flexible and Fast Estimation of Binary Merger Population Distributions with Adaptive KDE

JAM SADIQ,<sup>1</sup> THOMAS DENT,<sup>1</sup> AND DANIEL WYSOCKI<sup>2</sup>

<sup>1</sup>*Instituto Galego de Física de Altas Enerxías, Universidade de Santiago de Compostela, Santiago de Compostela, Galicia, Spain*

<sup>2</sup>*University of Wisconsin—Milwaukee, Milwaukee, Wisconsin, USA*

## ABSTRACT

The LIGO Scientific, Virgo and KAGRA Collaborations recently released GWTC-3, significantly expanding the number of gravitational wave (GW) signals. To address the – still uncertain – formation channels of these compact objects we require a range of methods to characterize their population properties. The computational cost of the Bayesian hierarchical methods employed thus far scales with the size of the event catalogs, and such methods have until recently assumed fixed functional forms for the source distribution. Here we propose a fast and flexible method to reconstruct the population of LIGO–Virgo merging black hole (BH) binaries without such assumptions. For sufficiently high event statistics and sufficiently low individual event measurement error (relative to the scale of population features) a kernel density estimator (KDE) reconstruction of the event distribution will be accurate. The method we propose improves the accuracy and flexibility of kernel density estimation for finite event statistic using an adaptive bandwidth KDE (awKDE). We apply awKDE to publicly released parameter estimates for 44 BH binary mergers reported with a false alarm rate below 1/yr in GWTC-2, in combination with a fast polynomial fit of search sensitivity, to obtain a non-parametric estimate of the mass distribution, and compare to Bayesian hierarchical methods. We also demonstrate a robust peak detection algorithm based on awKDE and use it to calculate the significance of the apparent peak in the BH mass distribution around 35  $M_{\odot}$ . We find such a peak is very unlikely to have occurred if the true distribution is a featureless power-law (significance of  $3.2\sigma$  for confident GWTC-2 BBH events).

*Keywords:* adaptive kde — compact binaries

## 1. INTRODUCTION

Advanced LIGO’s and Virgo’s (Aasi et al. 2015; Acernese et al. 2015) first three observing runs have produced many tens of confident detections of binary compact object mergers via gravitational wave (GW) emission, catalogued in GWTC-1 (Abbott et al. 2019), GWTC-2 (Abbott et al. 2021), GWTC-2.1 (Collaboration & Collaboration 2021), and GWTC-3 (Abbott et al. 2021a).<sup>1</sup> A detailed investigation of the population properties of binary black hole (BBH) mergers, the most commonly detected source type, has been published in Abbott et al. (2020) focusing on several population characteristics including their component masses and spins. This investigation was updated recently in Abbott et al. (2021b)

for GW observations up to the end of the O3 run, as catalogued in GWTC-3.

One objective has been to reconstruct the primary mass distribution of merging BBH, in order to address questions in stellar evolution, BH formation and binary formation channels. The primary BH masses have lower measurement uncertainty compared to other parameters such as binary spins, thus their distribution is expected to yield significant information which may eventually be compared with astrophysical model predictions. The binary chirp mass  $\mathcal{M} \equiv (m_1 m_2)^{3/5} (m_1 + m_2)^{-1/5}$ , where  $m_{1,2}$  are the source binary masses, is also measurable with (relatively) high precision, though a more complex function, thus it may also be considered for comparison with models that explicitly account for binary dynamics (e.g. Broekgaarden et al. 2021; Dominik et al. 2015).

In Abbott et al. (2020) specific functional forms and Bayesian hierarchical analysis are used to infer the mass distribution of binary mergers from these observed gravitational wave events: see Figure 1 for one output of such inference. These methods are well established, but as

Corresponding author: Jam Sadiq  
[jam.sadiq@usc.es](mailto:jam.sadiq@usc.es)

<sup>1</sup> Each successive catalog update includes previous detections.

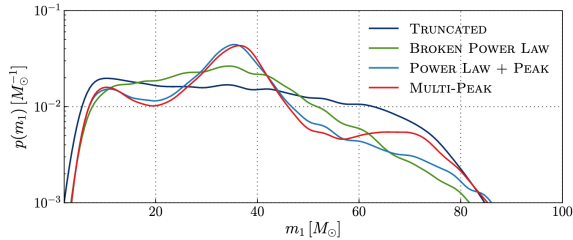


**Figure 1.** Observed primary black hole mass distribution predicted by each mass model in Abbott et al. (2020); reproduced from that publication.

our observed sample grows with future observing runs, both computational cost and modeling complexity will increase accordingly.

In this paper we propose a fast and flexible method for reconstructing binary merger population distributions via adaptive **kernel density estimation** (KDE), using a publicly available code (Menne 2020). This method addresses the same goals as the parametric hierarchical analyses, but without assuming any functional form of the distribution. A standard KDE with a fixed (global) bandwidth is unlikely to give an accurate representation of the BBH mass distribution, due to its complexity. Instead, we consider an adaptive KDE (awKDE) method to address the bandwidth problem and estimate the mass distribution of binary mergers from observed events. This method will validate and check the model assumptions of the standard Bayesian analyses in a flexible and computationally efficient way, and can potentially discover features not described by parametric models. The awKDE estimate of the detected event distribution also yields a differential merger rate estimate, using a fit of the search sensitivity as in Wysocki et al. (2019).

There is an apparent peak around  $35M_{\odot}$  in the primary mass distribution of observed GW events, as seen in the POWER LAW + PEAK (Talbot & Thrane 2018) and MULTI PEAK model results in Abbott et al. (2020) (see Fig. 1). In this work we also propose a method to determine the significance of one or more prominent peaks in the detected distribution, quantifying the probability that comparable statistical fluctuations might occur in the presence of selection effects. We thus introduce a new peak detection algorithm and apply it to GWTC-2 events. Investigating the presence and significance of such peaks will further help towards understanding BH binary formation; for instance, it has been suggested that pair-instability dynamics in supernovae could induce similar features in the BH mass function (recent discussions include Farmer et al. 2019; Baxter

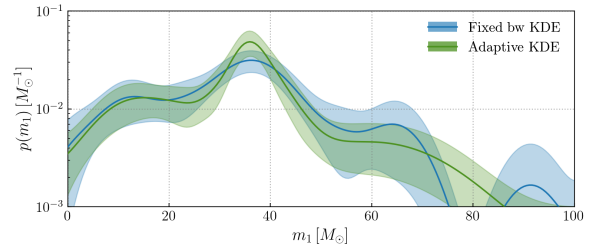


**Figure 2.** Fixed global bandwidth versus awKDE reconstruction of primary BH masses using GWTC-2 detected events.

et al. 2021; Woosley & Heger 2021) however as yet no definite signature has been identified.

The paper is organized as follows. In Section 2 we describe the awKDE algorithm and application to GW event detections. In Section 3 we apply awKDE to reconstruct the BBH mass distribution from the observed LVK events. In Section 4 we describe our peak detection algorithm and give results for GWTC-2 and preliminary results of GWTC-3 detected events and in Section 5 we summarize our conclusions.

## 2. RECONSTRUCTION METHOD

We propose the use of a kernel density estimate with adaptive bandwidth selection for reconstructing the probability distribution of source parameters for compact binary mergers observed via GW. This method is non-parametric, straightforward to apply, and enables the identification of general features in the distributions that may be an important input in the astrophysical interpretation of the merging binary population. Other, more sophisticated and computationally demanding non-parametric methods have recently been described in Tiwari & Fairhurst (2021); Tiwari (2021); Veske et al. (2021); Rinaldi & Del Pozzo (2021); Edelman et al. (2021). While a KDE with fixed (global) bandwidth is known to be a suitable method to estimate a distribution close to a single Gaussian, the mass (and possibly also spin) distributions of BBH mergers appear to have a more complex structure, which we do not expect to be well reconstructed by a simple KDE. In particular, the primary and secondary mass distributions may be composed of several components with widely differing mass scales and densities (which have in some cases, e.g. Talbot & Thrane (2018), been modelled by power laws and Gaussian peaks). Thus, we consider an extension where the bandwidth varies locally according to an initial estimate of the density of sample points (Terrell & Scott 1992; Sain & Scott 1996). The differences between a fixed global bandwidth KDE and our proposed awKDE are illustrated in Figure 2.

The fixed bandwidth KDE overestimates the width (underestimates the height) of the observed peak around  $35 M_\odot$ , but also yields a probably unphysical gap in the estimated distribution around  $80 M_\odot$ ; these undesirable aspects arise because a fixed bandwidth cannot both reconstruct small-scale features in regions with a high density of points, and supply enough smoothing to avoid artefacts in low density regions.

An adaptive bandwidth KDE (Wang & Wang 2011) is implemented in the open source code AWKDE (Menne 2020). We first describe the construction of a KDE from sample values  $X_i$ ,  $i = 1 \dots n$ : for instance,  $X_i$  may be a measured property of a binary merger. Later, we will describe how measurement uncertainties in these individual event properties are incorporated.

The algorithm computes a density estimate  $\hat{f}$  via

$$\hat{f}(x) = n^{-1} \sum_{i=1}^n \frac{1}{h\lambda_i} K\left(\frac{x - X_i}{h\lambda_i}\right), \quad (1)$$

where  $K(\cdot)$  is the standard Gaussian kernel,

$$K(z) = \frac{1}{\sqrt{2\pi}} \exp\left(-\frac{z^2}{2}\right), \quad (2)$$

$n$  is the total number of samples and, in general, the product  $h\lambda_i$  takes the role of a local bandwidth with  $h$  being the global bandwidth.

The first step is the computation of a pilot estimate  $\hat{f}_0$  setting  $\lambda_i = 1$  for all  $i$ , which is a standard fixed bandwidth KDE. Based on the pilot density  $\hat{f}_0$ , the local bandwidth accounting for variations in the density of samples is obtained via

$$\lambda_i = \left(\frac{\hat{f}_0(X_i)}{g}\right)^\alpha, \quad (3)$$

where  $\alpha$  is the local bandwidth sensitivity parameter ( $0 < \alpha \leq 1$ ) and  $g$  is a normalization factor

$$\log g = n^{-1} \sum_{i=1}^n \log \hat{f}_0(X_i). \quad (4)$$

Finally the adaptive KDE  $\hat{f}(x)$  is obtained by evaluating (1) with the variable (local) bandwidth  $h\lambda_i$ .

The above method assumes one-dimensional data  $X_i$ ; the method may also be applied to two- or more-dimensional data by linearly transforming the data to have zero mean and unit covariance.

The method requires a choice of the initial global bandwidth  $h$  and sensitivity parameter  $\alpha$ : we use the *leave-one-out cross-validation* method (Hastie et al. 2001) to determine these values. As a figure of merit for

the cross-validation we use the (log) likelihood,

$$\log \mathcal{L}_{\text{LOO}} = \sum_{i=1}^n \log \hat{f}_{\text{LOO},i}(X_i), \quad (5)$$

where  $\hat{f}_{\text{LOO},i}$  is the KDE constructed from all samples *except*  $X_i$ . We employ a grid search over a range of  $h$  and  $\alpha$  values; however, we often find the likelihood is maximized with  $\alpha$  at or close to 1, thus in some cases we will impose  $\alpha = 1$  rather than conduct the full 2d grid search.

### 2.1. Application to GW observations

The component masses of observed GW binary mergers have significant measurement uncertainties, which we wish to incorporate in reconstructions of the mass distribution. The parameters of each binary are obtained by Bayesian inference using models of the emitted GW waveform (e.g. Veitch et al. 2015), referred to as parameter estimation (PE). We consider detected mergers labelled by  $i = 1 \dots n$ : uncertainties in a given parameter  $X$  are quantified via random values  $X_i^k$  drawn from the posterior of the  $i$ th merger. Typically, some thousands of parameter samples are available per merger event (LVC 2020).

Although we use a random selection of PE samples for the KDE including measurement uncertainty, to first obtain the optimum global bandwidth and sensitivity parameter  $\alpha$  we evaluate the likelihood  $\mathcal{L}_{\text{LOO}}$  using only the *median* parameter value for each merger as the data  $X_i$ . This choice reduces the computational cost and avoids over-fitting of random fluctuations: note that these medians are independent values, whereas the PE samples for a given event  $i$ ,  $X_i^k$ , are not independent of one other, as they are all correlated with the (unknown) true source mass.

Having obtained the optimal  $h$  and  $\alpha$  choices, we construct the population KDE using 100 randomly chosen samples for each event. As noted above, in most cases the optimum  $\alpha$  is found at or close to 1, thus we often fix  $\alpha = 1$  for convenience. We also verify that increasing the number of PE samples in constructing the population KDE did not change our results significantly. We note that for large measurement errors relative to the scale of structures in the underlying distribution, the KDE result is likely to be over-dispersed, i.e., any sudden variations in the actual density will be smoothed out.<sup>2</sup>

<sup>2</sup> In principle this bias can be tackled by the computationally demanding hierarchical methods, if they model functional forms that are sufficiently close to the real distribution.

We also compute an uncertainty estimate (confidence interval) for the population KDE using the *bootstrap* technique (Efron 1979). Our major source of uncertainty lies in the finite number of binary merger events and the resulting count fluctuations in the estimate at a given parameter value. We account for this uncertainty by bootstrap resampling *over the merger events  $i$* : i.e., each bootstrap iteration contains some number of copies of the PE samples for each event  $i$ , with the number of copies approximately following a Poisson distribution. We extract the median and 5th and 95th percentiles from 1000 bootstrap iterations to obtain the confidence interval at any given parameter value. By plotting all bootstrap KDEs we can also visually identify regions of high and low uncertainty.

### 2.2. Fast approximate uncertainty estimate

While constructing an awKDE with median parameter values from PE, or in general using one parameter value per event, we can obtain a rapid uncertainty estimate by considering the awKDE Gaussian kernel contributions due to observed events at any given parameter value  $x$ . These contributions or KDE coefficients are

$$c_k(x) = n^{-1} \frac{1}{h\lambda_k} K\left(\frac{x - X_k}{h\lambda_k}\right), \quad (6)$$

where  $k$  labels the observed events. We may estimate the standard deviation of the coefficients,  $\sigma_c$ , as

$$\sigma_c^2(x) \simeq \langle c_k^2 \rangle - \langle c_k \rangle^2, \quad (7)$$

where  $\langle \cdot \rangle$  represents the mean over observed events. As the KDE is the sum of  $n$  such coefficients its variance is a factor  $n$  larger, thus we take  $\sigma_{\text{KDE}}(x) = \sqrt{n}\sigma_c(x)$ . The resulting estimated 90% confidence interval is  $1.64\sigma_{\text{KDE}}(x)$  above and below the central value,<sup>3</sup> i.e.

$$\epsilon_{\text{KDE}}(x) = 1.64\sqrt{n}\sigma_c(x). \quad (8)$$

We compare this estimate with the bootstrap uncertainty region and find them in a good agreement for most parameter values, as shown in Figure 3. Clearly this direct variance estimate is computationally much more efficient than the bootstrap.

While this coefficient-based estimate agrees with the bootstrap for small bandwidths (relative to the range of sample values  $X_i$ ), for large values of bandwidth it becomes significantly smaller than the bootstrap uncertainty. While we do not have a complete explanation

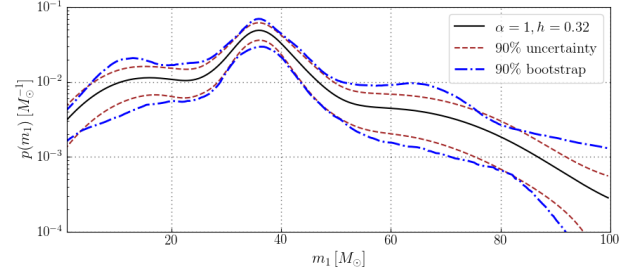


**Figure 3.** awKDE (black solid line) for GWTC-2 events with error estimates using a standard bootstrap method (blue dot-dashed lines) and from the Gaussian Kernel coefficients from awKDE code (brown dashed lines) using Eq. (8). The two error estimates are in good agreement for most parameter values.

of this behaviour, we may get some insight from simple approximate arguments. First, our coefficient-based estimate does not account for any systematic variation in the coefficients due to changes in the bandwidths  $\lambda_k$  between different data realizations.

Proceeding heuristically, we approximate the Gaussian kernel coefficients at a given  $x$  as constants  $c_L$  (‘large’ coefficients) for  $n_L$  data points  $X_k$  ‘close’ to  $x$  relative to their bandwidths  $h\lambda_k$ , and vanishing for the remaining  $n - n_L$  points ‘far away’ from  $x$ . Then the KDE coefficient-based error estimate is approximately  $(c_L n_L / n) \sqrt{n_L^{-1} - n^{-1}}$ . This corresponds to the variance of a binomial distribution with a success rate  $n_L / n$ . When the bandwidths are large,  $n_L$  will be close to  $n$  (many events will have large and near-equal coefficients), leading to a cancellation.

However, given that the data are produced by an underlying Poisson process, as the total number of astrophysical events observed is not fixed, we also considered a modified estimate which scales with the variance of the count of ‘close’ events, reducing to  $(c_L n_L / n) \sqrt{n_L^{-1}}$ . This corresponds to removing the second term in Eq. (7), i.e.

$$\hat{\sigma}_c^2(x) = \langle c_k^2 \rangle. \quad (9)$$

With this modified estimate, the corresponding 90% error  $\hat{\epsilon}_{\text{KDE}}(x)$  agrees much more closely with the bootstrap uncertainties for large bandwidths. This property motivates our use of  $\hat{\epsilon}_{\text{KDE}}$  in the peak detection method to be introduced in Section 4.

## 3. AWKDE POPULATION RECONSTRUCTION FROM LIGO-VIRGO DETECTIONS

Here we apply these methods to reconstruct the distribution of parameters for BBH observed in the O1, O2 and O3a runs (Abbott et al. 2019, 2021). As in Abbott et al. (2020), we consider significant events (false alarm

<sup>3</sup> The factor 1.64 corresponds to the 95th percentile of the standard normal distribution.



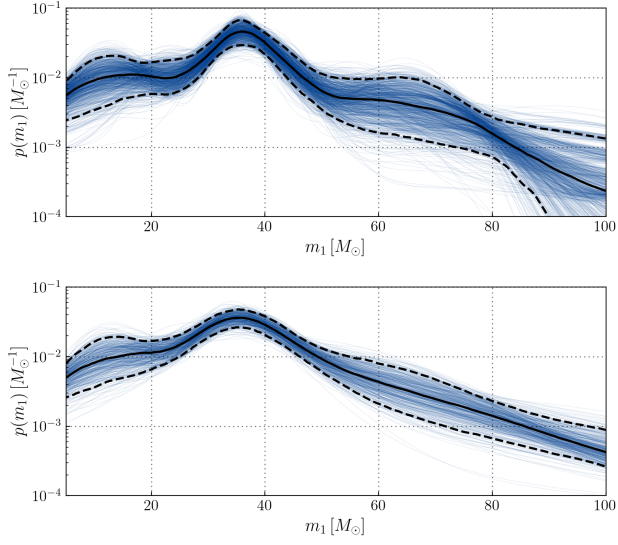


**Figure 4.** KDE with uncertainty estimates of source frame primary mass,  $m_1$ , for detected BBH events in the O1, O2 and O3a observing runs. Top: KDE using the PE sample median for each event. Bottom: KDE constructed using 100 random samples from each observed event. The median (black solid), 90% confidence interval (black dashed lines) and blue curves are constructed using a bootstrap. Our KDE results match closely the POWER LAW + PEAK (Talbot & Thrane 2018) and MULTI PEAK model results in (Abbott et al. 2020), see Fig. 1.

rate below 1/yr) for which both component masses are below  $3 M_\odot$ , finding 44 such mergers. We first consider the primary mass  $m_1$  defined in the binary source frame. The resulting KDE bootstrap samples, median estimate and 90% confidence intervals are shown in Figure 4, where the top panel uses only the median  $m_1$  value for each binary merger and the lower panel accounts for measurement uncertainties via the PE samples. These primary mass distributions match well those inferred using parametric models in Abbott et al. (2020), specifically with the POWER LAW + PEAK (Talbot & Thrane 2018) and MULTI PEAK models most preferred by the GWTC-2 data. We note that there is a clear global maximum in the observed distribution at  $\sim 35 M_\odot$  and that the uncertainty in the mass distribution is smallest here. The awKDE is also able to reconstruct a wide dynamic range of densities without excessive statistical uncertainties.

As an alternative to the primary mass, we also consider the chirp mass  $\mathcal{M}$  for observed BBH mergers, which is also measured with relatively small uncertainty. The corresponding KDEs are shown in Figure 5. Here in addition to the expected peak just below  $30 M_\odot$  we note hints of a secondary peak around  $\mathcal{M} \simeq 10$ , though small compared to the estimated uncertainties: however,

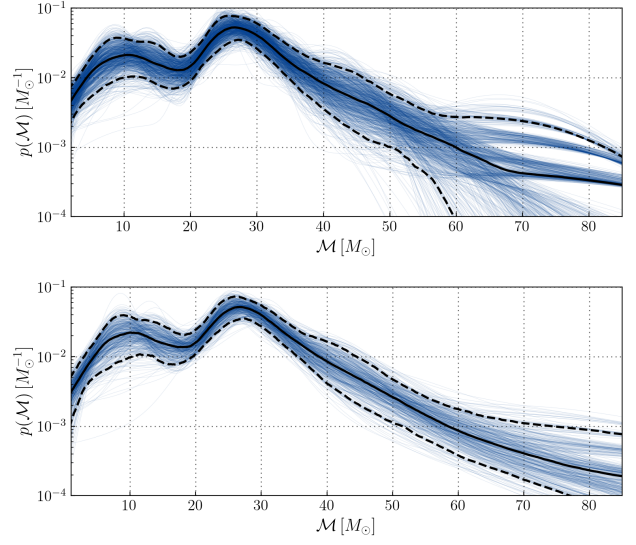


**Figure 5.** KDE with uncertainty estimates of source chirp mass,  $\mathcal{M}$ , for detected events in the O1, O2 and O3a observing runs. Top: KDE using the PE sample median for each event. Bottom: KDE constructed using 100 random samples from each observed event. The median (black solid), 90% confidence interval (black dashed lines) and blue curves are constructed using a bootstrap. In addition to the principal peak in the distribution around  $25\text{--}30 M_\odot$ , there is a hint of further structure around  $10 M_\odot$ .

with this data we are not able to distinguish the multiple peaks claimed in Tiwari & Fairhurst (2021) from random fluctuations.

We also used recently available public data from GWTC-3 (Abbott et al. 2021a) to construct the distribution of primary and chirp masses using PE samples for confident BBH events, and find new features in the distributions consistent with the results in Abbott et al. (2021b). As with the GWTC-2 data, we do not recover significant structure beyond the two visible peaks. The peak at  $35\text{--}40 M_\odot$  in primary mass ( $25\text{--}30 M_\odot$  in chirp mass) shows signs of asymmetry (skewness) relative to a locally Gaussian form, which may indicate a need for more complex models.

### 3.1. Merger rate estimation from awKDE

We also consider estimation of BBH merger rates using our awKDE results. The additional ingredient in this analysis is the sensitive volume  $V$  within which a source is detectable: we quantify this based on an approximation for the sensitivity of GW detectors, with corrections to account for the actual behaviour of searches in real data (Wysocki et al. 2019). The idea is to calibrate a semi-analytic function  $VT_{\text{analytic}}$  against the re-weighted result of injections (i.e. simulated signals added to real data and analyzed by search pipelines)  $VT_{\text{inj}}$ , assuming

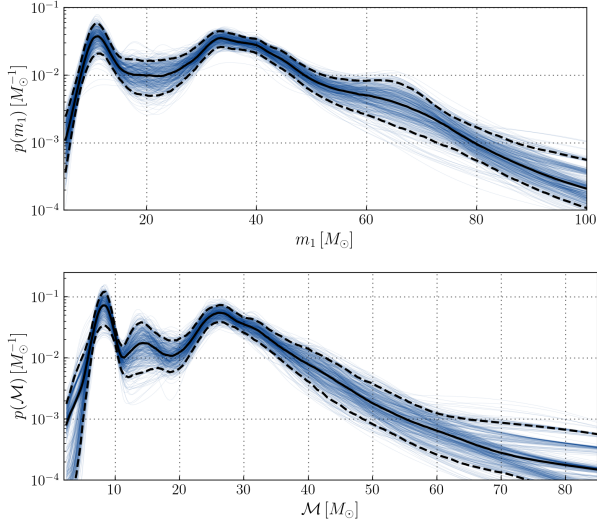


**Figure 6.** Application of awkDE to GWTC-3 data (Abbott et al. 2021a): we reconstruct the source primary mass  $m_1$  and chirp mass  $\mathcal{M}$  distributions, seeing additional features at lower masses consistent with the results in Abbott et al. (2021b).

a parameterized relationship between them that can be expressed via basis functions.

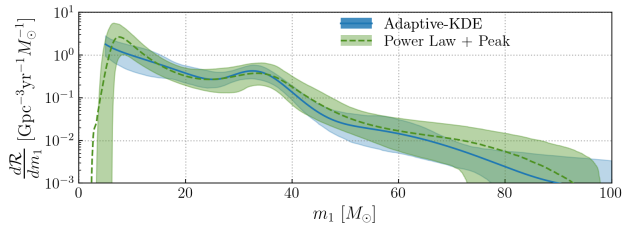


**Figure 7.** Rate estimates using adaptive KDE and sensitive volume for BBH events in GWTC-2. The green band curve is the rate estimate using the POWER LAW + PEAK model from Abbott et al. (2020); the blue band shows a rate estimate using KDE results from median PE values and a fit to search sensitivity.

For the O1-O2 and O3a observing runs, the ‘uncalibrated’ semi-analytic sensitivity is estimated using the criterion that the signal-to-noise ratio (SNR) of a signal in the second most sensitive detector, using specific reference power spectral densities, should be greater than 8. This semi-analytic estimate  $VT_{\text{analytic}}$  is obtained for a given observing time  $T$  over a grid of intrinsic source parameters such as component masses. For the injection  $VT_{\text{inj}}$ , one performs a set of injections and counts the number detected by search pipelines to obtain an average  $VT_{\text{inj}}$  for the injected population at given intrinsic parameters. The calibrated estimate of  $VT$  is then obtained by fitting a correction function to the deviations

of  $VT_{\text{inj}}$  from  $VT_{\text{analytic}}$ , as described in Wysocki (2020) and applied in Abbott et al. (2020).

We compute the merger rate density using this corrected  $VT$  and our KDE results for the primary mass  $\hat{f}(m_1)$  from observations up to O3a. We obtain  $VT(m_1)$  assuming a power law mass distribution for the secondary  $m_2$ , taking the median value, 1.26, of the power-law parameter  $\beta_q$  from Abbott et al. (2020), and find the merger rate density via

$$\frac{dR}{dm_1} = n \frac{\hat{f}(m_1)}{VT(m_1)}. \quad (10)$$

Our estimate is in good agreement with the results in Abbott et al. (2020) for the POWER LAW + PEAK model, as shown in Fig. 7.

### 3.2. 2D KDE for cosmological evolution of BH mass distribution

We apply our adaptive KDE in a two-dimensional space using median PE values for  $m_1$  in the source frame and luminosity distance  $D_L$  for BBH events in GWTC-2, following the same procedure of leave-one-out cross-validation to determine the optimal global bandwidth and sensitivity parameter. As shown in Figure 8, the resulting two-dimensional KDE shows peaks around  $35 M_\odot$ , similar to the one-dimensional mass KDEs; these overdensities appear to be present consistently over different distances. Although the number of events is cur-

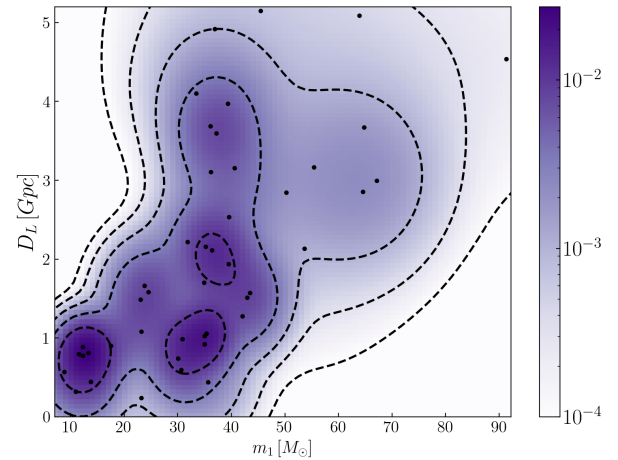


**Figure 8.** Adaptive KDE over the source frame primary mass and luminosity distance of parameters for BBH events in GWTC-2. The feature around  $35 M_\odot$  appears to be present consistently at different distances.

rently too small to draw specific conclusions, the method may be useful in the near future to investigate or check features in the cosmological distribution.

#### 4. DETECTION OF BH MASS FUNCTION PEAKS WITH AWKDE

In this section we describe our algorithm to detect the prominent peaks in our BH mass function with awkDE. Peaks in the mass spectrum can provide hints of the formation channels responsible for the observed BBH. As shown in Figure 1, the two parameterised models of Abbott et al. (2020) that allow for a Gaussian peak component find such a feature around  $35 M_\odot$ , which is also visible in the awkDE results. However, the statistical preference for such models over power-law based models with no peak component is only moderate (log10 Bayes factor  $< 2$  for GWTC-2 events). Here we pursue an alternative strategy by developing a general technique to identify peaks in the mass function, and a procedure to estimate their statistical significance.

##### 4.1. Peak Detection Algorithm

We are proposing an algorithm for the detection of most prominent peak in any given distribution (in one dimension), which we then apply to our adaptive width KDEs. In order to detect the most prominent peak we consider the following algorithm.

- For a given population fit  $\hat{f}(x)$ , find all local maxima, denoted  $\{x_j^p\}$ .
- Using a chosen window size  $\delta$  (examples provided later), evaluate the PDF on either side of the peak,  $\hat{f}_j^\pm = \hat{f}(x_j^p \pm \delta)$ . In the event that  $x_k^p \pm \delta$  is outside of our training set, to avoid extrapolation we substitute  $\hat{f}_j^+$  ( $\hat{f}_j^-$ ) with the value of  $\hat{f}$  at the highest (lowest) training point.
- Compute peak heights using

$$H_j^p = \hat{f}(x_j^p) - (\hat{f}_j^- + \hat{f}_j^+)/2. \quad (11)$$

- Evaluate the estimated uncertainty at each peak,  $\epsilon_j^p$ , in our case defined in Equation 8
- Determine the most significant peak by maximizing a detection statistic, which combines  $H_j^p$  and  $\epsilon_j^p$  (examples provided later).

Figure 9 demonstrates the detection algorithm for BH primary masses.

*Mock data sets and algorithm tuning*—In order to evaluate and optimize the detection performance of our algorithm we created several large-scale mock datasets, each having 10,000 samples with 60 data points in each sample: then based on the detection statistic values produced by the algorithm for background and signal samples, we

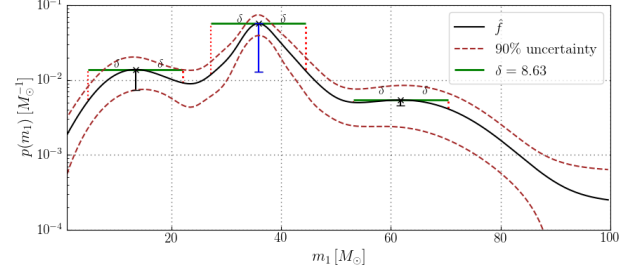


**Figure 9.** Peak detection algorithm for KDEs applied for BH primary masses in GWTC-2 with an arbitrary choice of global bandwidth  $h$ . The solid black curve is the awkDE estimate  $\hat{f}$  with the dashed brown curves indicating 5th and 95th percentile uncertainties estimated via Eq. (8). Green line, the window size  $\delta$  to get  $\hat{f}_j^\pm$ , with the vertical red dotted lines indicate the construction used to measure peak height, while blue (black) vertical lines indicate the most significant (less significant) peak height.

calculate ROCs to measure the efficiency of peak detection.

For a signal detection, we construct a mock dataset containing a peak, referred to as the Peak dataset, containing samples which include a uniform component and a Gaussian component. Each of the sample contain uniformly distributed random data points from a truncated power law, a fraction (random choices range from 10% to 100%) of data points drawn from a Gaussian distribution with random choice of Gaussian mean (ranges  $10 M_\odot$  to  $52 M_\odot$ ) and standard deviation (ranges from  $10 M_\odot$  to  $40 M_\odot$ ).

For the background we construct three different datasets to test the performance of our algorithm. The first is a ‘Uniform’ dataset having uniform random samples, which are the simplest realisation of a null case with no peak feature. The two other background datasets are drawn from a truncated power law distribution of primary and secondary masses of BBH systems, using fixed/varying (mean/all values of hyperparameters used in TRUNCATED MASS (Talbot & Thrane 2017) model in Abbott et al. (2020)) and also pass a survival test given real data sensitive volume related semi-analytic  $VT_{\text{analytic}}$  calibration. They are called fixed/variable hyperparameter power law VT corrected (FPLVT/V-PLVT) datasets. Note that we have in total 7460 different choices of varying hyperparameters so we have a total of 7460 samples rather than 10,000 samples in VPLVT dataset.

Using these three mock datasets as background and a detection statistic from the Peak dataset we compute ROCs as shown in Figure 11. Our figure of merit is the ROC, i.e. true positive rate, at a false alarm probability (FAP) of  $10^{-3}$ . We use this criterion to tune the fixed

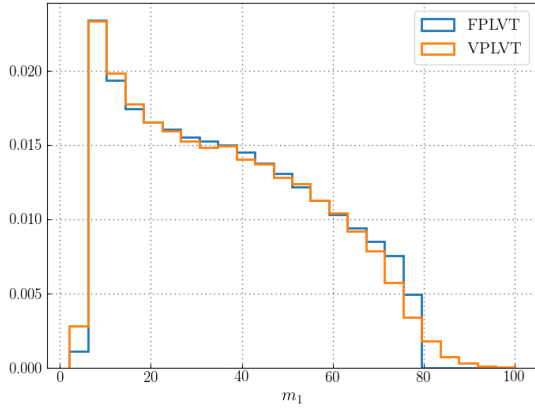


**Figure 10.** Distribution of background data with fixed/variable hyperparameter power law VT corrected (FPLVT/VPLVT) datasets.

window size  $\delta$  in peak algorithm, the choice of optimized bandwidth in awKDE for samples in mock datasets, and choices of peak detection statistic.

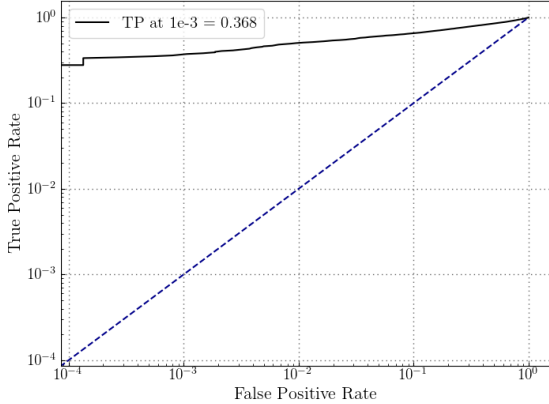


**Figure 11.** ROC curve with background VPLVT dataset and signal Peak dataset for an arbitrary choice of detection statistic. The curve shows that our peak algorithm gives 36.8% success at false alarm probability of  $10^{-3}$  for these mock datasets.

*Tuning  $\delta$  for peak height*—In our algorithm we need to choose fixed window size  $\delta$  to compute the height of each peak. In our first experiment we use fixed  $\delta$  values, trying the values  $\{10, 20, 30, 40, 50\} M_{\odot}$ . We find that ROC curves with choices in the range of  $20 M_{\odot}$  to  $40 M_{\odot}$  gives promising results. For the second experiment we used  $\delta = kh$ , where  $h$  is the standard deviation of the Gaussian kernel used to construct the initial pilot (fixed bandwidth) KDE, i.e. the global bandwidth: we used

constant factors  $k$  ranging from 1 to 8 to determine  $\delta$ . From the ROCs resulting from our experiments, we find that the choice  $\delta = kh$  performs better than the fixed  $\delta$  choices. Another advantage of  $\delta = kh$  vs fixed  $\delta$  is that the awKDE bandwidth  $h$  is automatically scaled by the covariance of the data, whereas fixed  $\delta$  would have to be retuned when applying the method to other physical situations.

*Tuning criteria for optimized bandwidth*—In order to find optimized bandwidth we are not using leave-one-out cross validation for peak analysis as for 10,000 datasets this is a computationally expensive task. Also, the optimal bandwidth for accurate reconstruction of the mass distribution is not necessarily most suited to detection of peaks. Instead, we construct an awKDE for each of the sample in datasets fixing  $\alpha = 1$ , for several different choices of bandwidth. Out of these different bandwidth KDEs for a given sample, we select the one for which the maximum peak detection statistic is highest.

*Use of bounded awKDE with 10% range of data-points*—In order to check any specific trends in our algorithm we plotted several diagnostics tests including peak height, peak detection statistic and peak location for our mock datasets. From these diagnostic studies we find out that using awKDE without bounds can lead to some artifact in peak detections for the peaks at the edges of awKDE as there are less contributions of data points at these edges of KDEs. This is a known artifact in awKDE as explained in Hoy & Raymond (2021a,b), so we use bounded KDE rather than unbounded one to avoid any issue due to edges of KDE and our bounded KDE increases the ROC at low FAP. Furthermore, we find out that the range of values of data-points on which we construct our awKDE can also effect the performance of our peak detections. The best choice of minimum and maximum of the range of data-points for awKDE are the one that use 10% of the minimum and maximum value of sample values in each sample of mock datasets.

*Tuning choice of peak detection statistic*—We lastly require to specify the detection statistic which determines the most significant peak in each awKDE. We considered various possibilities: the simplest choice would be to use the peak height  $H_j^p$ , however we also investigated combinations of the peak height and the error estimate  $\epsilon_{\text{KDE}}(x_j^p)$  by checking the performance of our peak detection algorithm using ROCs. We first used the maximum of all heights in a awKDE as a detection statistic which can be a good first choice but since these peaks in an awKDE are computed using a choice of  $\delta$  and bandwidth that can lead to some artifacts in maximum peak heights which can be non-astrophysical so we also tried



other choices. To reduce the artifacts due to both the optimized bandwidth, and  $\delta$  we use error estimates as in Eq. (8)  $\epsilon_{\text{KDE}}(x_j^p)$  at the peak as computed from awkKDE and define ratio  $H_j^p/\epsilon_{\text{KDE}}(x_j^p)$  as our detection statistic and compute ROCs. From our diagnostic tests, we find out that this new peak detection statistic favors the choice of lower values of optimized bandwidth for background dataset and can affect our algorithm. Finally, to avoid artefacts at high bandwidth we consider a modified uncertainty estimate as in Eq. (9): using this choice  $H_j^p/\hat{\epsilon}_{\text{KDE}}(x_j^p)$  the ROCs are increased further, thus this is our final choice of detection statistic.

*Optimized detection choice*—After the tuning steps described above, our choice of peak detection statistic is the ratio  $H_j^p/\hat{\epsilon}_{\text{KDE}}(x_j^p)$ : for both the FPLVT and VPLVT datasets  $\delta = 2h$  gives the highest ROCs. Hence we use these choices to compute the FAP of the result of applying the algorithm to a real dataset consisting of observed GW signals from BBH merger.

#### 4.2. Peak detection for GWTC-2 BBH events

With our optimized detection choice, we apply it to the 44 high-significance BBH detections in O1, O2 and O3a as used in Abbott et al. (2020): we find a peak detection statistic of 2.72. To assess the significance of this value we construct comparable background samples, each having 44 data points, using VT corrected samples that take into account all hyperparameters for primary mass distributions. So we use all hyperparameters used in O1, O2 and O3a observing runs (Abbott et al. 2020) to compute datasets of 7640 samples. We then compute the FAP for the actual detections up to O3a using this background datasets, obtaining a value 0.0006 ( $3.2\sigma$  significance). Thus, the apparent feature in GWTC-2 BBH primary component masses is very unlikely to have originated from random fluctuations if the true underlying distribution was a power law. This result strengthens the motivation to search for possible astrophysical explanations of such features.

## 5. CONCLUSIONS

We introduce a fast and efficient method of using awkKDE to get binary merger population distributions. This method can be used for sanity checks for computational extensive models for binary merger population distributions. This method can use PE sample values of each event and take into account uncertainty estimates. These awkKDE results can be used for rate estimates. While we have demonstrated its use for mass and distance distributions, it can be extended to higher dimensions given more observational results. In addition we introduce a robust peak detection algorithm and demonstrate that this algorithm can detect the most prominent in a given distribution.

## ACKNOWLEDGEMENT

This material is based upon work supported by NSF’s LIGO Laboratory which is a major facility fully funded by the National Science Foundation. The authors are grateful for computational resources provided by the LIGO Laboratory and supported by National Science Foundation Grants PHY-0757058 and PHY-0823459. This research has made use of data, software and/or web tools obtained from the Gravitational Wave Open Science Center (<https://www.gw-openscience.org/>), a service of LIGO Laboratory, the LIGO Scientific Collaboration and the Virgo Collaboration. LIGO Laboratory and Advanced LIGO are funded by the United States National Science Foundation (NSF) as well as the Science and Technology Facilities Council (STFC) of the United Kingdom, the Max-Planck-Society (MPS), and the State of Niedersachsen/Germany for support of the construction of Advanced LIGO and construction and operation of the GEO600 detector. Additional support for Advanced LIGO was provided by the Australian Research Council. Virgo is funded, through the European Gravitational Observatory (EGO), by the French Centre National de Recherche Scientifique (CNRS), the Italian Istituto Nazionale di Fisica Nucleare (INFN) and the Dutch Nikhef, with contributions by institutions from Belgium, Germany, Greece, Hungary, Ireland, Japan, Monaco, Poland, Portugal, Spain.

## REFERENCES

- Aasi, J., et al. 2015, *Class. Quant. Grav.*, 32, 074001, doi: [10.1088/0264-9381/32/7/074001](https://doi.org/10.1088/0264-9381/32/7/074001)
- Abbott, B. P., et al. 2019, *Phys. Rev. X*, 9, 031040, doi: [10.1103/PhysRevX.9.031040](https://doi.org/10.1103/PhysRevX.9.031040)
- Abbott, R., et al. 2020. <https://arxiv.org/abs/2010.14533>
- . 2021, *Phys. Rev. X*, 11, 021053, doi: [10.1103/PhysRevX.11.021053](https://doi.org/10.1103/PhysRevX.11.021053)
- . 2021a. <https://arxiv.org/abs/2111.03606>
- . 2021b. <https://arxiv.org/abs/2111.03634>
- Acernese, F., et al. 2015, *Class. Quant. Grav.*, 32, 024001, doi: [10.1088/0264-9381/32/2/024001](https://doi.org/10.1088/0264-9381/32/2/024001)
- Baxter, E. J., Croon, D., McDermott, S. D., & Sakstein, J. 2021, *Astrophys. J. Lett.*, 916, L16, doi: [10.3847/2041-8213/ac11fc](https://doi.org/10.3847/2041-8213/ac11fc)

- Broekgaarden, F. S., et al. 2021.  
<https://arxiv.org/abs/2112.05763>
- Collaboration, L. S., & Collaboration, V. 2021, GWTC-2.1: Deep Extended Catalog of Compact Binary Coalescences Observed by LIGO and Virgo During the First Half of the Third Observing Run - Candidate Data Release, v2, Zenodo, doi: [10.5281/zenodo.5117970](https://doi.org/10.5281/zenodo.5117970)
- Dominik, M., Berti, E., O’Shaughnessy, R., et al. 2015, *Astrophys. J.*, 806, 263, doi: [10.1088/0004-637X/806/2/263](https://doi.org/10.1088/0004-637X/806/2/263)
- Edelman, B., Doctor, Z., Godfrey, J., & Farr, B. 2021.  
<https://arxiv.org/abs/2109.06137>
- Efron, B. 1979, *The Annals of Statistics*, 7, 1 .  
<https://doi.org/10.1214/aos/1176344552>
- Farmer, R., Renzo, M., de Mink, S. E., Marchant, P., & Justham, S. 2019, doi: [10.3847/1538-4357/ab518b](https://doi.org/10.3847/1538-4357/ab518b)
- Hastie, T., Tibshirani, R., & Friedman, J. 2001, *The Elements of Statistical Learning*, Springer Series in Statistics (New York, NY, USA: Springer New York Inc.)
- Hoy, C., & Raymond, V. 2021a, Bounded KDEs.  
[https://lscsoft.docs.ligo.org/pesummary/unstable\\_docs/core/bounded\\_kdes.html](https://lscsoft.docs.ligo.org/pesummary/unstable_docs/core/bounded_kdes.html)
- . 2021b, *SoftwareX*, 15, 100765, doi: [10.1016/j.softx.2021.100765](https://doi.org/10.1016/j.softx.2021.100765)
- LVC. 2020, GWTC-2 Data Release: Parameter Estimation Samples and Skymaps,  
<https://dcc.ligo.org/LIGO-P2000223/public/>
- Menne, T. 2020, awkDE code,  
<https://github.com/mennthor/awkde>
- Rinaldi, S., & Del Pozzo, W. 2021.  
<https://arxiv.org/abs/2109.05960>
- Sain, S. R., & Scott, D. W. 1996, *Journal of the American Statistical Association*, 91, 1525.  
<https://www.tandfonline.com/doi/abs/10.1080/01621459.1996.10476720>
- Talbot, C., & Thrane, E. 2017, *Phys. Rev. D*, 96, 023012, doi: [10.1103/PhysRevD.96.023012](https://doi.org/10.1103/PhysRevD.96.023012)
- . 2018, *Astrophys. J.*, 856, 173, doi: [10.3847/1538-4357/aab34c](https://doi.org/10.3847/1538-4357/aab34c)
- Terrell, G. R., & Scott, D. W. 1992, *The Annals of Statistics*, 20, 1236 .  
<https://doi.org/10.1214/aos/1176348768>
- Tiwari, V. 2021, *Class. Quant. Grav.*, 38, 155007, doi: [10.1088/1361-6382/ac0b54](https://doi.org/10.1088/1361-6382/ac0b54)
- Tiwari, V., & Fairhurst, S. 2021, *Astrophys. J. Lett.*, 913, L19, doi: [10.3847/2041-8213/abfbc7](https://doi.org/10.3847/2041-8213/abfbc7)
- Veitch, J., et al. 2015, *Phys. Rev. D*, 91, 042003, doi: [10.1103/PhysRevD.91.042003](https://doi.org/10.1103/PhysRevD.91.042003)
- Veske, D., Bartos, I., Márka, Z., & Márka, S. 2021.  
<https://arxiv.org/abs/2105.13983>
- Wang, B., & Wang, X. 2011, Bandwidth Selection for Weighted Kernel Density Estimation.  
<https://arxiv.org/abs/0709.1616>
- Woosley, S. E., & Heger, A. 2021, *Astrophys. J. Lett.*, 912, L31, doi: [10.3847/2041-8213/abf2c4](https://doi.org/10.3847/2041-8213/abf2c4)
- Wysocki, D. 2020, Calibrating semi-analytic VT’s to injections in O3a,  
<https://dcc.ligo.org/LIGO-T2000432/public>
- Wysocki, D., Lange, J., & O’Shaughnessy, R. 2019, *Physical Review D*, 100.  
[http://dx.doi.org/10.1103/PhysRevD.100.043012](https://dx.doi.org/10.1103/PhysRevD.100.043012)